Transmission-Line Analysis of a Capacitively Coupled Microstrip-Ring Resonator

Cheng-Cheh Yu, *Member, IEEE*, and Kai Chang, *Fellow, IEEE*

***Abstract*— The resonant frequencies of a microstrip-ring resonator capacitively coupled to a feed line are accurately analyzed using a transmission-line model. By making use of $ABCD$- and Y-admittance matrices, a compact closed-form expression for the input impedance of the ring alone is analytically derived and shows that the ring can be equivalently viewed as a frequency-dependent capacitor. The coupling gap is then modeled by an equivalent L-network comprising a parallel and a series gap capacitance obtained by modifying Garg and Bahl's closed-form expressions for an end-to-end microstrip gap. By simplifying the parallel and series combinations of the overall equivalent circuit, the total input impedance looking from the feed line to the gap is analytically derived to predict the resonant frequencies. To verify the analysis, the resonant frequencies of the capacitively coupled ring resonator have been accurately measured, with the experimental results showing very good agreement with the theoretical predictions.**

***Index Terms*— Microstrip-ring resonator, resonant frequency, transmission-line analysis.**

I. Introduction

MICROSTRIP resonators have been widely used for the measurements of dispersion, phase velocity [1]–[4], dielectric constant [5], and discontinuities [6], [7]. The two configurations that are most often used are linear and ring resonators. For the linear resonator, the fringing fields on both open ends will cause a foreshortening effect [8]–[10], and surface- and space-wave radiation losses [11]–[13], whereas the ring resonator shown in Fig. 1 has two advantages: it is free of open-ended effects and its curvature effects can be made negligible if its diameter is large enough, with respect to the linewidth [14]. A review of ring circuits can be found in [15].

A microstrip-ring structure resonates when its electrical length is about an integral multiple of the guide wavelength. The size of the coupling gap determines the coupling degree between the feed line and the ring resonator. Most of the studies on ring resonators in the open literatures use rigorous, but sophisticated, field theory to analyze their electrical characteristics and do not include the effects of the coupling gap between the feed line and the ring resonator [16]–[19]. Due to the field interactions in the coupling-gap region, the actual resonant frequency will have some deviation from that of a stand-alone microstrip-ring resonator. To simplify the analysis, Chang *et al.* [20] first proposed a straightforward, but reasonably accurate transmission-line method that can include the gap discontinuities and devices mounted along the ring. In Chang's work, a π-network is used to model the coupling gap. Scrutiny of the overall equivalent circuit reveals that there will be an extra capacitance parallel-connected to the ring as the gap size goes to infinity. Therefore, a better circuit representation for the gap is needed.

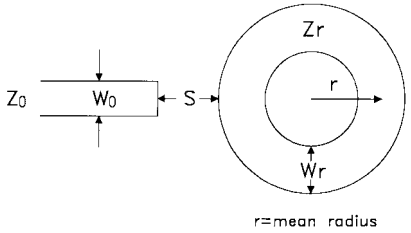

Fig. 1. The microstrip-ring resonator capacitively coupled to a microstrip feed line.

In the following sections, a compact closed-form expression for the input impedance of an isolated microstrip-ring resonator will be analytically derived by making use of $ABCD$ and Y-admittance matrices. In addition, instead of the π-network used in [20], a more reasonable L-network will be given to model the coupling gap without changing the original ring structure. Then the overall equivalent circuit model for the capacitively coupled ring resonator, including the coupling gap effects, will be derived to predict the existing resonant frequencies. Finally, accurate measurements will be performed to verify the validity of the analysis given in this paper.

II. Input Impedance of a Stand-Alone Microstrip-Ring Resonator

A microstrip line formed as a closed loop on a dielectric substrate, which resonates at certain frequencies, is shown in Fig. 2. If the inner and outer radii of the isolated ring resonator do not differ too much from each other, then the microstrip ring may have the same dispersion characteristics as those for the linear one. Thus, it can be analyzed by viewing it as a microstrip line that ends on itself [15].

Manuscript received December 26, 1996; revised July 18, 1997.

C.-C. Yu is with the Department of Electrical Engineering, Texas A&M University, College Station, Texas 77843-3128 USA, on leave from the Department of Electronic Engineering, National Taipei Institute of Technology, Taipei, Taiwan, R.O.C.

K. Chang is with the Department of Electrical Engineering, Texas A&M University, College Station, TX 77843–3128 USA.

Publisher Item Identifier S 0018-9480(97)08021-6.

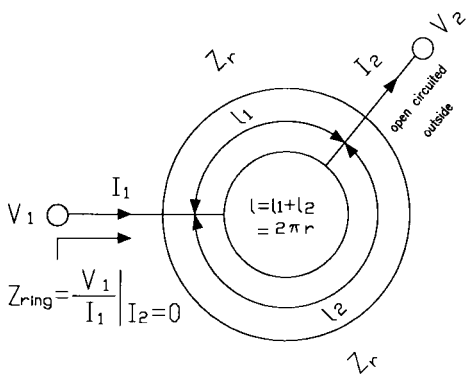

Fig. 2. Transmission-line model of a stand-alone microstrip-ring resonator.

In order to derive an equation for the input impedance of the ring resonator with a mean circumference $\ell = 2\pi r$, the ring resonator is conceptually split into two sections, as shown in Fig. 2. With both ends of the two split sections connected together, port one is used to designate the feeding port and port two is arbitrarily chosen and kept open-circuited outside, since there is nothing connected there. By resorting to the well-established transmission-line theory, the $ABCD$ transfer matrices for the individual sections can be given as follows [21, pp. 231–244]:

$$\begin{bmatrix} A & B \\ C & D \end{bmatrix}_{1,2} = \begin{bmatrix} \cos\beta_r\ell_{1,2} & jZ_r\sin\beta_r\ell_{1,2} \\ jY_r\sin\beta_r\ell_{1,2} & \cos\beta_r\ell_{1,2} \end{bmatrix} \tag{1}$$

where subscripts 1 and 2 refer to the split transmission-line sections of lengths ℓ_1 and ℓ_2, $Z_r = 1/Y_r =$ the characteristic impedance of the microstrip ring that forms the ring resonator, and $\beta_r =$ the corresponding propagation constant.

The Y-admittance matrices for the upper and lower sections can then be obtained from the $ABCD$ matrices (as shown below) by performing the matrix transformation given in [21, pp. 231–244]:

$$\begin{bmatrix} Y_{11} & Y_{12} \\ Y_{21} & Y_{22} \end{bmatrix}_{1,2} = \begin{bmatrix} -jY_r\cot\beta_r\ell_{1,2} & +jY_r\csc\beta_r\ell_{1,2} \\ +jY_r\csc\beta_r\ell_{1,2} & -jY_r\cot\beta_r\ell_{1,2} \end{bmatrix}. \tag{2}$$

Since both ends of the two split transmission-line sections are connected in parallel, the individual Y-matrices are added to give the resultant Y-matrix shown in (3) at the bottom of the page. Moreover, due to the fact that port two is actually open-circuited outside, it can be readily shown that the input admittance seen at port one is

$$Y_{\text{ring}} = \frac{Y_{11}Y_{22} - Y_{12}Y_{21}}{Y_{22}}. \tag{4}$$

Therefore, the required input impedance of the isolated ring resonator can be obtained as shown in (5), at the bottom of the page, where r and ℓ are the mean radius and circumference of the ring, respectively.

As can be seen from (5), the input impedance of the ring resonator has been expressed in a general compact closed form. The equation is similar to that given in [22], but the steps taken are not provided there.

In order to develop an equivalent circuit for the ring resonator alone, the Z_{ring} in (5) is rewritten as

$$Z_{\text{ring}} = \frac{1}{j\omega C_{\text{ring}}} \tag{6}$$

then

$$C_{\text{ring}} = \frac{2Y_r[1-\cos(2\pi\beta_r r)]}{\omega\sin(2\pi\beta_r r)} \tag{7}$$

where ω is the radian frequency (rad/s).

Equations (6) and (7) indicate that the microstrip-ring resonator alone can be formally viewed as a simple frequency-dependent capacitor which may become inductive as the operating frequency increases. Hereafter, owing to this equivalence, the ring resonator will be represented by the capacitance given in (7).

III. Equivalent Circuit for the Coupling Gap and the Total Input Impedance

A. Equivalent Circuit for the Coupling Gap

The coupling gap in Fig. 1 is a challenging discontinuity problem to solve because it cannot be reduced to a two-dimensional problem. In this paper, the coupling gap of the resonator will be modeled by an equivalent L-network, comprising a parallel and a series gap capacitances C_p and C_g, as shown in Fig. 3. The suitability of this equivalence for

$$\begin{bmatrix} Y_{11} & Y_{12} \\ Y_{21} & Y_{22} \end{bmatrix}_{\text{ring}} = \begin{bmatrix} -jY_r(\cot\beta_r\ell_1 + \cot\beta_r\ell_2) & +jY_r(\csc\beta_r\ell_1 + \csc\beta_r\ell_2) \\ +jY_r(\csc\beta_r\ell_1 + \csc\beta_r\ell_2) & -jY_r(\cot\beta_r\ell_1 + \cot\beta_r\ell_2) \end{bmatrix}. \tag{3}$$

$$\begin{aligned} Z_{\text{ring}} &= \frac{Y_{22}}{Y_{11}Y_{22} - Y_{12}Y_{21}} \\ &= \frac{-jY_r(\cot\beta_r\ell_1 + \cot\beta_r\ell_2)}{[-jY_r(\cot\beta_r\ell_1 + \cot\beta_r\ell_2)]^2 - [jY_r(\csc\beta_r\ell_1 + \csc\beta_r\ell_2)]^2} \\ &= -j\frac{Z_r}{2}\left.\frac{\sin\beta_r\ell}{1-\cos\beta_r\ell}\right|_{\ell=\ell_1+\ell_2} = -\frac{Z_r}{2}\left.\frac{\sin(2\pi\beta_r r)}{1-\cos(2\pi\beta_r r)}\right|_{2\pi r=\ell} \end{aligned} \tag{5}$$

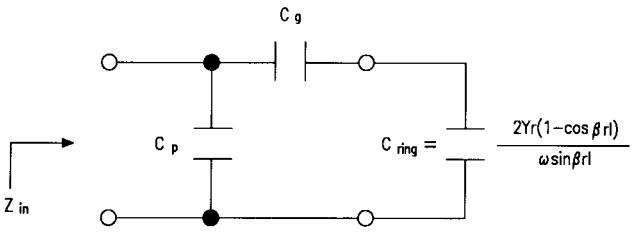

Fig. 3. The equivalent lumped circuit for the microstrip-ring resonator including the coupling gap.

the coupling gap can be justified by the following lines of reasoning.

- When the gap size goes to infinity in Fig. 1, the series gap capacitance will approach zero. The microstrip-ring resonator will then be isolated and left unchanged if the two-capacitance L-network in Fig. 3 is used for the coupling gap. Therefore, the adoption of the equivalent L-network for the gap is reasonable.
- If a three-capacitance π-network is used to model the coupling gap in Fig. 1, as done in [20], there will be one extra capacitance parallel connected to the ring resonator as the gap size becomes infinitely large. This means that the original structure of the ring resonator will be changed somewhat by adopting the three-capacitor π-network. Therefore, the two-capacitor L-network in Fig. 3 is a more reasonable simulation than the three-capacitor π-network used in [20] for modeling the coupling gap between the feed line and the resonator.

B. Total Input Impedance for the Capacitively Coupled Microstrip-Ring Resonator

In Section II, the input impedance of a stand-alone ring resonator has been shown to be equivalent to a frequency-dependent capacitor when viewed as a microstrip line that ends on itself. Moreover, based on the physical explanation in Section III-A, the coupling gap between the feed line and the resonator can be better modeled by a two-capacitor L-network. Therefore, the overall equivalent circuits for the capacitively coupled ring resonator can now be integrated together to form a single-port three-capacitor network, as depicted in Fig. 3. Obviously the total equivalent circuit is simple and easy to use. The total input capacitance C_{in} and impedance Z_{in} are readily obtained, as shown in (8) at the bottom of the page, and

$$Z_{\text{in}} = jX_{\text{in}} = \frac{1}{j\omega C_{\text{in}}}. \tag{9}$$

By definition, the resonant frequency for a circuit is the frequency that makes the total input impedance purely resistive as seen by the source. In other words, the capacitively coupled microstrip-ring resonator in Fig. 1 resonates when $X_{\text{in}} = 0$.

C. Calculation of the Parallel and Gap Capacitances for the Coupling Gap

The parallel and series gap capacitances used to model the coupling gap in this paper are assumed to take the same values as that for an end-to-end microstrip gap [23]. An extensive analysis of this gap has led to comprehensive results which work for tightly coupled gaps. Among various field calculations, Benedek and Silvester's work using a rigorous charge reversal method [24] seems to be the most reliable one, as judged by comparing it with many independent measurements published in the literatures. In this paper, Garg and Bahl's closed-form expressions [25] will be modified by curve-fitting the available numerical results in [24] to give the capacitances for C_p and C_g, shown in Fig. 3.

When applying Garg and Bahl's closed-form expressions to calculate the even-mode capacitance C_{even} and odd-mode capacitance C_{odd} to give C_p and C_g, it can be shown that there is an obvious jump in the capacitance distribution for different gap sizes. In addition, there are some discrepancies between their results and Benedek and Silvester's data for dielectric substrates of small ε_r. In this paper, Garg and Bahl's expressions have been modified to alleviate the aforementioned jump in the capacitance-versus-gap size curves and to lead to a better match with the numerical results obtained by Benedek and Silvester for dielectric substrates of small ε_r. The modified equations for C_p and C_g calculations are given below:

$$\frac{C_{\text{even}}(\varepsilon_r = 9.6)}{W_0} = 12\left(\frac{S}{W_0}\right)^{m_e} e^{k_e} \quad \text{(pF/m)} \tag{10}$$

$$\frac{C_{\text{odd}}(\varepsilon_r = 9.6)}{W_0} = \left(\frac{S}{W_0}\right)^{m_0} e^{k_0} \quad \text{(pF/m)} \tag{11}$$

where

$$m_e = 0.8675, \qquad k_e = 2.043\left(\frac{W_0}{h}\right)^{0.12}, \quad 0.1 \le S/W_0 \le 0.5 \tag{12a}$$

$$m_e = \frac{1.565}{\left(\frac{W_0}{h}\right)^{0.16}} - 1, \qquad k_e = 1.97 - \frac{0.03}{\left(\frac{W_0}{h}\right)}, \quad 0.5 \le S/W_0 \le 1.0 \tag{12b}$$

$$m_0 = \frac{W_0}{h}\left(0.619 \log_{10}\frac{W_0}{h} - 0.3853\right), \quad 0.1 \le S/W_0 \le 1.0 \tag{12c}$$

$$k_0 = 4.26 - 1.453 \log_{10}\frac{W_0}{h}, \qquad 0.1 \le S/W_0 \le 1.0 \tag{12d}$$

$$\begin{aligned} C_{\text{in}} &= \frac{C_p C_g + C_p C_{\text{ring}} + C_g C_{\text{ring}}}{C_g + C_{\text{ring}}} \\ &= \frac{C_p\{\omega C_g \sin(2\pi\beta_r r) + 2Y_r[1 - \cos(2\pi\beta_r r)]\} + 2C_g Y_r[1 - \cos(2\pi\beta_r r)]}{\omega C_g \sin(2\pi\beta_r r) + 2Y_r[1 - \cos(2\pi\beta_r r)]} \end{aligned} \tag{8}$$

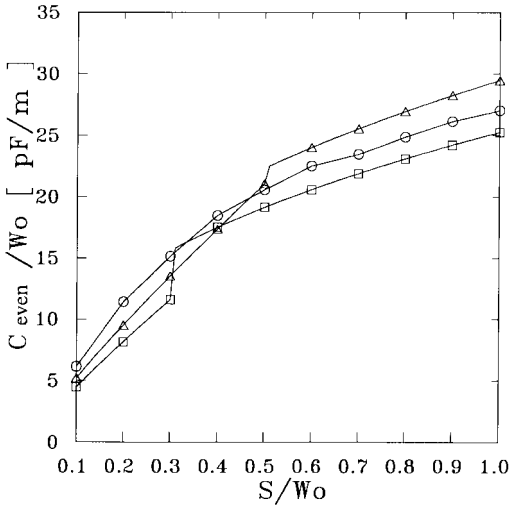

Fig. 4. Even-mode capacitances for the end-to-end microstrip coupling gap with $\varepsilon_r = 2.5$, and $W_0/h = 2.0$. ∘ obtained by Benedek and Silvester [24], □ by Garg and Bahl [25], and Δ by (10)–(16).

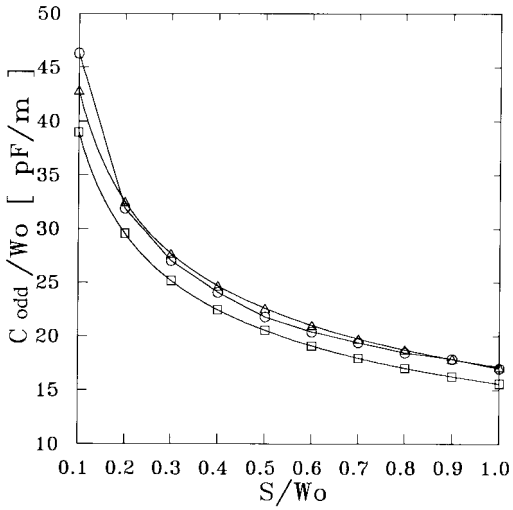

Fig. 5. Odd-mode capacitances for the end-to-end microstrip coupling gap with $\varepsilon_r = 2.5$ and $W_0/h = 2.0$. ∘ calculated by Benedek and Silvester [24], □ by Garg and Bahl [25], and Δ by (10)–(16).

and

$$C_{\text{even}}(\varepsilon_r) = 1.167 C_{\text{even}}(\varepsilon_r = 9.6)(\varepsilon_r/9.6)^{0.9} \quad (13)$$

$$C_{\text{odd}}(\varepsilon_r) = 1.1 C_{\text{odd}}(\varepsilon_r = 9.6)(\varepsilon_r/9.6)^{0.8} \quad (14)$$

$$C_p = \frac{C_{\text{even}}}{2} \quad (15)$$

$$C_g = \frac{2C_{\text{odd}} - C_{\text{even}}}{4} \quad (16)$$

where h and ε_r are the thickness and dielectric constant of the substrate, respectively.

The modifications were made in the limits of S/W_0 in (12a) and (12b), and the coefficients in (13) and (14). In order to justify the above modifications, two examples are given below to examine the differences among the results obtained by Benedek and Silvester [24], Garg and Bahl [25], and the modified version of Garg and Bahl's formulas, as shown in (10)–(16) for dielectric substrates of small ε_r.

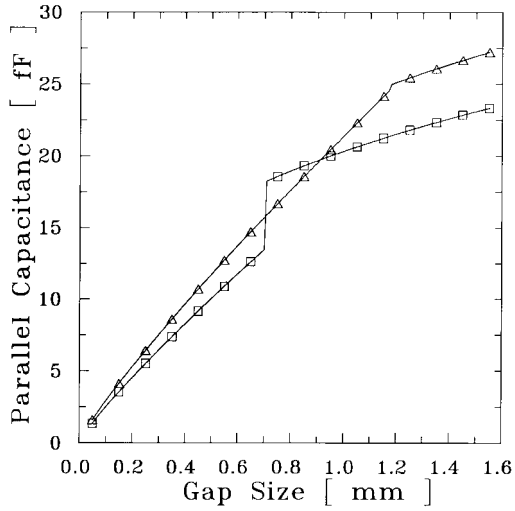

Fig. 6. Parallel capacitances for the end-to-end microstrip coupling gap with $\varepsilon_r = 2.2$, $h = 31$ mil $= 0.7874$ mm, and $W_0 = 2.3495$ mm. □ obtained by using Garg and Bahl's formulas [25], and Δ by (10)–(16).

Example 1: **Subject:** Calculation of even- and odd-mode capacitances for end-to-end microstrip gap.

Parameters: Substrate dielectric constant $= \varepsilon_r = 2.5$, microstrip linewidth/substrate thickness $= W_0/h = 2.0$, gap size/microstrip linewidth $= S/W_0$ varied from 0.1 to 1.0.

Results: The calculated even- and odd-mode capacitance distributions versus S/W_0 are shown in Figs. 4 and 5, respectively. As can be clearly seen from Fig. 4, the even-mode capacitance distribution obtained by using (10)–(16) has a small discontinuity at $S/W_0 = 0.5$, while that calculated by utilizing the original Garg and Bahl's formulas has a much bigger jump at $S/W_0 = 0.3$. Additionally close inspection of Figs. 4 and 5 shows that the results given by Benedek and Silvester are better approximated by the modified expressions given in (10)–(16) for dielectric substrates of smaller ε_r.

Example 2: **Subject:** Calculation of parallel and gap capacitances for end-to-end microstrip gap.

Parameters: Substrate dielectric constant $= \varepsilon_r = 2.2$, substrate thickness $= h = 31$ mil $= 0.7874$ mm, microstrip linewidth $= W_0 = 2.3495$ mm, gap size $= S$ varied from 0.05 to 1.55 mm.

Results: The calculated parallel and series capacitances are shown in Figs. 6 and 7, respectively. Once again, the curves obtained by using the modified equations given in (10)–(16) are smoother than those obtained by the original Garg and Bahl's formulas.

As justified by the comparisons made in the preceding two examples, the modified version of Garg and Bahl's formulas hereafter will be used to calculate the parallel and gap capacitances for the microstrip coupling gap in Fig. 1.

IV. Theoretical and Experimental Results for the Study of Gap Effects

To verify the validity of the transmission-line analysis for a capacitively coupled microstrip-ring resonator developed in

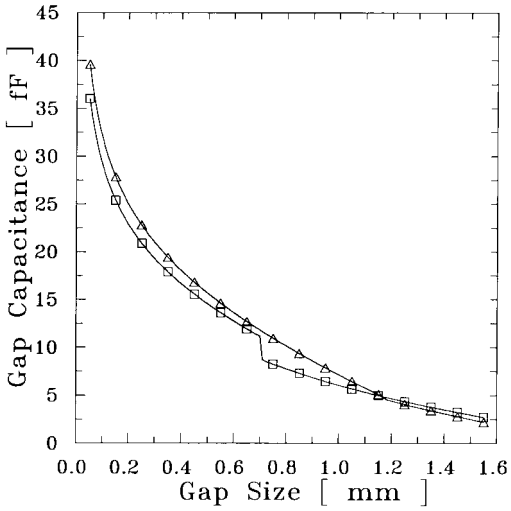

Fig. 7. Series capacitances for the end-to-end microstrip coupling gap with $\varepsilon_r = 2.2$, $h = 31$ mil $= 0.7874$ mm, $W_0 = 2.3495$ mm, and $\square$ calculated by using Garg and Bahl's formulas [25], and Δ by (10)–(16).

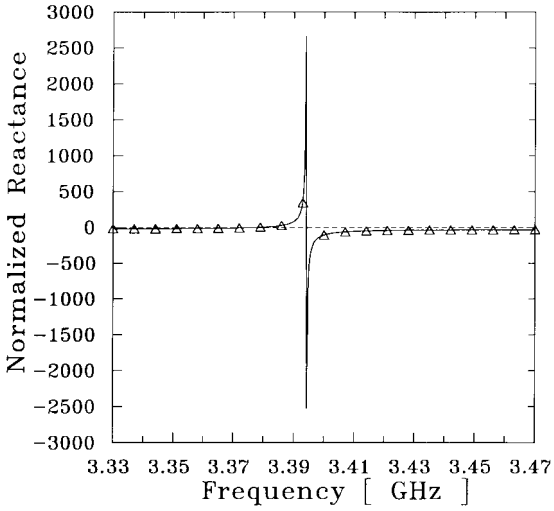

Fig. 8. The theoretical normalized total input reactance X_{in}/Z_0 versus frequency by using (6)–(16) for a ring resonator.

Sections II and III, experimental data have been taken and compared to the theoretical predictions. The parameters used are described as follows:

1) substrate material: RT/Duroid 5880 with $\varepsilon_r = 2.2 \pm 0.02$, substrate thickness $= h = 0.7874$ mm, copper thickness $= t = 0.03556$ mm, and substrate loss tangent $= \tan\ \delta = 0.0009$;
2) parameters of feed-in microstrip line: $W_0 = 2.3495$ mm, $Z_0 = 50.444\ \Omega$, $\varepsilon_{\text{eff},0} = 1.865$, and $\beta_0 = \omega\sqrt{\varepsilon_{\text{eff},0}}/c = \omega\sqrt{1.865}/3 \times 10^8$ (as calculated by the widely used microwave software LineCalc[1]);
3) parameters for the line that forms the microstrip-ring resonator: $W_r = W_0$, $Z_r = Z_0$, $\varepsilon_{\text{eff},r} = \varepsilon_{\text{eff},0}$, $\beta_r = \beta_0$, and $r = 10.2959$ mm;
4) coupling gap size $= S$ varied from 0.1 to 0.9 mm;
5) coax-to-microstrip connector: MFR-FSCM-61 697 (SMA connector from M/A-COM with protruding inner conductor made flat).

By using (6)–(16), the theoretical total input reactances can be plotted as a function of frequencies. The normalized reactances X_{in}/Z_0 for the aforementioned capacitively coupled microstrip-ring resonator with 0.1-mm gap size have been calculated and is shown in Fig. 8. It can be seen that the resonator has both a series resonant frequency f_s and a parallel resonant frequency f_p, resembling the characteristics of a stable piezoelectric quartz crystal [26]. This suggests that microstrip-ring resonators may find useful applications in narrow-band circuit designs.

The solution of (9) for satisfying the resonance condition $X_{\text{in}}(\omega_r) = 0$ is merely a root-finding problem. There are several canonical methods available to solve this problem in numerical analysis. Each method has its own advantages and disadvantages. In view of the drastic reactance change around the series and parallel resonant frequencies (as shown in Fig. 8), the bisection method has been utilized for the subsequent analysis. Although other methods may offer greater rates of convergence to the point nearest to the given initial guess, they cannot converge unless the function is well-behaved.

Additionally, during the process of deriving the input impedance of the ring resonator alone, it has been assumed that the ring resonator is lossless. However, there will always be some accompanying dielectric, conductor, and even radiation losses. From the circuit theory on lumped-element resonators [21, pp. 330–336], the quality factor Q is defined as (series inductive reactance/series resistance) for a series resonant circuit and (parallel resistance/parallel inductive reactance) for a parallel one. Therefore, there will be a small series resistance seen by the source for a high-Q resonator at the series resonant frequency and a maximum parallel resistance at the parallel resonance point.

When performing the experiments and measuring the resulting fundamental resonant frequency with a network analyzer, it can be easily seen that the resonant condition $X_{\text{in}}(\omega_r) = 0$, corresponds to a minimum S_{11} scattering parameter as long as there is some loss existing in the tested circuit. It is because the field is excited to the largest extent at the resonant frequency and, hence, the loss reaches its maximum value. This method of measuring the resonant frequency by spotting the dip in $S_{11}(\omega)$ is referred to as the reflection measurement [7].

The theoretical simulation for coupling gap size ranging from 0.05 to 0.95 mm has been carried out, and the corresponding circuit experiments with gap sizes varied from 0.1 to 0.9 mm have been carefully implemented and measured using an HP 8510B automated network analyzer. The network analyzer is the ramp source selected for circuit excitation and a 801-point single-port S_{11} calibration has been done between 3.37 and 3.40 GHz. Both the theoretical and experimental results are shown together in Fig. 9. The results show that the theoretical resonant frequencies using the preceding modified ring circuit analysis agree very well with the measurements. Therefore, the transmission-line model and analysis presented

[1] LineCalc, EEsof, Inc., Westlake Village, CA, 1993.

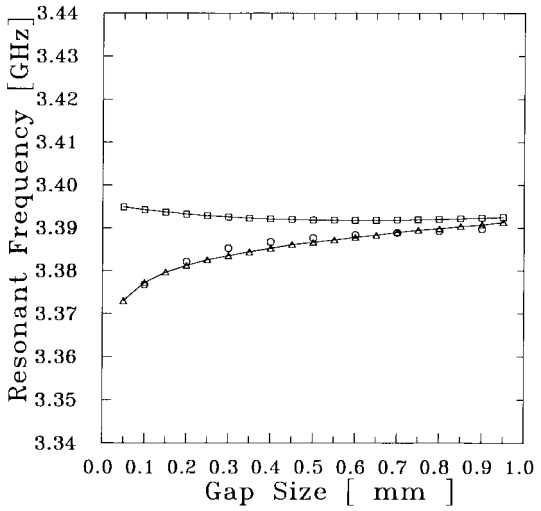

Fig. 9. Fundamental resonant frequencies as a function of coupling gap sizes for a ring resonator. The line with Δ represents the theoretical series resonant frequency, the $\square$ represents the theoretical parallel resonance points, and the $\circ$ represents the experimental results.

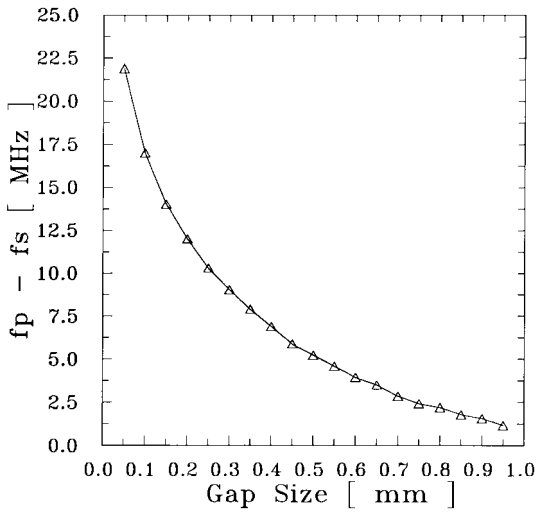

Fig. 10. Difference between the theoretical series and parallel resonant frequencies as a function of coupling gap sizes with the same circuit parameters used in Fig. 9.

in this paper are accurate. Close inspection of Fig. 9 reveals the following discoveries.

1) The measured resonant frequencies are in closer agreement with the theoretical series resonant frequencies than the parallel ones. This can be attributed to the following fact. A small series resistance representing the loss for a high-Q resonant circuit matches the system characteristic impedance (50 Ω) better at series resonance, while the parallel resonance exhibits a maximum parallel resistance that gives more mismatch. Thus, the series resonant modes are easier to be excited and, in turn, the measured return loss will be larger. Therefore, only the series resonant modes were observed in Fig. 9.
2) The coupling gap effects on the performance of the microstrip-ring resonator have to be taken into account, especially when a small gap is introduced. The field perturbations between the feed line and the ring resonator will cause the actual resonant frequency to have appreciable deviation from that of the isolated microstrip ring.
3) It is well known that a larger gap results in less field disturbance and, hence, less change in the resonant frequency. If the coupling gap effects on the resonant frequency are to be negligible, the ratio of the coupling size to the feed linewidth S/W_0 should be set no less than 0.4, as can be seen from the theoretical simulation and experiment results shown in Fig. 9.
4) As the size of the coupling gap is increased, the series and parallel resonance points become closer and closer. This suggests that the overall circuit Q of the capacitively coupled ring resonator will be increased as the coupling gap is made larger. The differences between the series resonant frequency f_s and parallel resonant frequency f_p have been calculated as a function of frequencies, as given in Fig. 10, which shows that there is a direct connection between the coupling gap size and the bandwidth. Like the piezoelectric quartz crystal [26], the ring resonator has close series and parallel resonance points. This implies that ring resonators may find important applications in designing narrow-band filters and high spectral-purity oscillators.

V. Conclusions

A transmission-line method is used to calculate the resonant frequency of a capacitively coupled microstrip-ring resonator, including the coupling gap. The theoretical predictions have been shown to agree very well with the experimental results. Summarized below are the main findings of this paper.

- By viewing the microstrip ring as a microstrip line that ends on itself, its input impedance has been analytically derived in a compact closed form and can be considered as a frequency-dependent capacitor.
- Instead of a π-network, the coupling gap between the microstrip feed line and the ring resonator has been more reasonably modeled by an L-network comprising a parallel and series gap capacitance.
- Combining the overall equivalent lumped circuits for the capacitively coupled microstrip-ring resonator, the total input impedance can be found from simple parallel and series combinations of three capacitances.
- For end-to-end microstrip coupling gap on dielectric substrates of small ε_r, Garg and Bahl's closed-form expressions for the related capacitance calculations have been modified to better fit Benedek and Silvester's widely cited results.
- The measured resonant frequencies for the capacitively coupled ring resonator agree better with the theoretical series resonances than the parallel resonance points.
- The ratio of the coupling gap size to the microstrip feed line should be set greater than 0.4 if the coupling gap effects on the resonant frequency are to be negligible. Otherwise, the gap effects should be included for accurate predictions of the resonant frequency.

ACKNOWLEDGMENT

The authors would like to thank H. Tehrani for his valuable suggestions and L. Fan for his technical assistance and circuit fabrication.

REFERENCES

[1] P. Troughton, "High Q-factor resonator in microstrip," *Electron. Lett.*, vol. 4, no. 24, pp. 520–522, Nov. 1968.
[2] P. Troughton, "Measurement techniques in microstrip," *Electron. Lett.*, vol. 5, no. 5, pp. 25–26, Jan. 1969.
[3] I. Wolff and N. Koppik, "Microstrip ring resonator and dispersion measurement on microstrip lines," *Electron. Lett.*, vol. 7, no. 26, pp. 779–781, Dec. 1971.
[4] C. Edwards, "Microstrip measurements," in *IEEE MTT-S Int. Microwave Symp. Dig.*, Dallas, TX, June 15–17, 1982, pp. 338–341.
[5] P. A. Bernard and J. M. Gautray, "Measurement of dielectric constant using a microstrip ring resonator," *IEEE Trans. Microwave Theory Tech.*, vol. 39, pp. 592–595, Mar. 1991.
[6] I. M. Stephenson and B. Easter, "Resonant techniques for establishing the equivalent circuits of small discontinuities in microstrip," *Electron. Lett.*, vol. 7, no. 19, pp. 582–584, Sept. 1971.
[7] W. J. R. Hoefer and A. Chattopadhyay, "Evaluation of the equivalent circuit parameters of microstrip discontinuities through perturbation of a resonant ring," *IEEE Trans. Microwave Theory Tech.*, vol. MTT-23, pp. 1067–1071, May 1975.
[8] A. Farrar and A. T. Adams, "Computation of lumped microstrip capacities by matrix methods—rectangular sections and end effect," *IEEE Trans. Microwave Theory Tech.*, vol. MTT-19, pp. 495–496, May 1971.
[9] L. S. Napoli and J. J. Hughes, "Foreshortening of microstrip open circuits on alumina substrates," *IEEE Trans. Microwave Theory Tech.*, vol. MTT-19, pp. 559–561, June 1971.
[10] D. S. James and S. H. Tse, "Microstrip end effects," *Electron. Lett.*, vol. 8, no. 2, pp. 46–47, Jan. 1972.
[11] E. J. Denlinger, "Losses of microstrip lines," *IEEE Trans. Microwave Theory Tech.*, vol. MTT-28, pp. 513–522, June 1980.
[12] P. B. Katehi and N. Alexopoulos, "Frequency-dependent characteristics of microstrip discontinuities in millimeter-wave integrated circuits," *IEEE Microwave Theory Tech.*, vol. MTT-33, pp. 1029–1035, Oct. 1985.
[13] R. W. Jackson and D. M. Pozar, "Full-wave analysis of microstrip open-end and gap discontinuities," *IEEE Trans. Microwave Theory Tech.*, vol. MTT-33, pp. 1036–1042, Oct. 1985.
[14] R. P. Owens, "Curvature effect in microstrip ring resonator," *Electron. Lett.*, vol. 12, no. 14, pp. 356–357, July 1976.
[15] K. Chang, *Microwave Ring Circuits and Antennas*. New York: Wiley, 1996, pp. 125–131.
[16] Y. S. Wu and F. J. Rosenbaum, "Mode chart for microstrip ring resonators," *IEEE Trans. Microwave Theory Tech.*, vol. MTT-21, pp. 487–489, July 1973.
[17] S. G. Pintzos and R. Pregla, "A simple method for computing the resonant frequencies of microstrip ring resonators," *IEEE Trans. Microwave Theory Tech.*, vol. MTT-26, pp. 809–813, Oct. 1975.
[18] A. K. Sharma and B. Bhat, "Spectral domain analysis of microstrip ring resonator," *Arch. Elek. übertragung.*, vol. 33, no. 3, pp. 130–132, Mar. 1979.
[19] V. K. Tripathi and I. Wolff, "Perturbation analysis and design equations for open-end closed-ring microstrip resonators," *IEEE Trans. Microwave Theory Tech.*, vol. MTT-32, pp. 405–409, Apr. 1984.
[20] K. Chang, S. Martin, F. Wang, and J. L. Klein, "On the study of microstrip ring and varactor-tuned ring circuits," *IEEE Trans. Microwave Theory Tech.*, vol. MTT-35, pp. 1288–1295, Dec. 1987.
[21] D. M. Pozar, *Microwave Engineering*. Reading, MA: Addison-Wesley, 1990.
[22] M. Makimoto and M. Sagawa, "Varactor tuned bandpass filters using microstrip-line resonators," in *1986 IEEE MTT-S Int. Microwave Symp. Dig.*, Baltimore, MD, June 2–4, pp. 411–414, 1986.
[23] K. C. Gupta, R. Garg, and I. J. Bahl, *Microstrip Lines and Slotline*. Norwood, MA: Artech House, 1979, pp. 132–136.
[24] P. Benedek and P. Silvester, "Equivalent capacitances for microstrip gaps and steps," *IEEE Trans. Microwave Theory Tech.*, vol. MTT-20, pp. 729–733, Nov. 1972.
[25] R. Garg and I. J. Bahl, "Microstrip discontinuities," *Int. J. Electron.*, vol. 45, pp. 81–87, 1978.
[26] I. M. Gottlieb, *Basic Oscillator*. New York: Rider, 1963.

Cheng-Cheh Yu (S'91–M'91) was born on January 1, 1964, in Taipei, Taiwan, R.O.C. He received the five-year-program diploma degree in electrical engineering from the National Taipei Institute of Technology, Taipei, Taiwan, R.O.C., in 1984, and the M.S. and Ph.D. degrees in electrical engineering from National Taiwan University, Taipei, Taiwan, R.O.C., in 1988 and 1991, respectively

From 1991 to 1992, he worked for the Telecommunication Laboratories of the Communications Ministry, Taiwan, R.O.C., as an Associate Researcher. He then joined the Department of Electronic Engineering, National Taipei Institute of Technology, where he has been the Director of the Electrooptics Research and Development Center (1994–1996), and is currently an Associate Professor. His professional interests include advanced electromagnetic theory, microwave circuits, antenna analysis/design, advanced computational electromagnetics, electronic communication techniques, and passive/active RF filter designs.

Dr. Yu is a member of the Institute of the Chinese Electrical Engineers (CIEE), and the American Radio Relay League (ARRL). He holds the R.O.C. Certificate of National Advanced Official Examination (1985). In 1996, he received the first position in the National Overseas Examination sponsored by the R.O.C. Educational Ministry, as well as having received research awards from the National Science Council (1993) and the National Taipei Institute of Technology (1996). In 1995, he was elected as one of the top 100 outstanding youths in Taiwan, R.O.C., and received the Special Achievement Award from the National Taipei Institute of Technology.

Kai Chang (S'75–M'76–SM'85–F'91) received the B.S.E.E. degree from the National Taiwan University, Taipei, Taiwan, R.O.C., in 1970, the M.S. degree from the State University of New York at Stony Brook, in 1972, and the Ph.D. degree from the University of Michigan at Ann Arbor, in 1976.

From 1972 to 1976, he worked as a Research Assistant for the Microwave Solid-State Circuits Group, Cooley Electronics Laboratory, University of Michigan. From 1976 to 1978, he was employed by Shared Applications, Inc., Ann Arbor, MI, where he worked in computer simulation of microwave circuits and microwave tubes. From 1978 to 1981, he worked for the Electron Dynamics Division, Hughes Aircraft Company, Torrance, CA, where he was involved in the research and development of millimeter-wave solid-state devices and circuits, power combiners, oscillators, and transmitters. From 1981 to 1985, he worked as a Section Head for the TRW Electronics and Defense, Redondo Beach, CA, developing state-of-the-art millimeter-wave integrated circuits and subsystems including mixers, VCO's, transmitters, amplifiers, modulators, upconverters, switches, multipliers, receivers, and transmitters. He then joined the Electrical Engineering Department, Texas A&M University, as an Associate Professor, was promoted to full Professor in 1988, and in 1990, was appointed E-Systems Endowed Professor of electrical engineering. He has authored and co-authored *Microwave Solid-State Circuits and Applications* (Wiley, 1994), *Microwave Ring Circuits and Antennas* (Wiley, 1996), and *Integrated Active Antennas and Spatial Power Combining* (Wiley, 1996), has served as editor for the four-volume *Handbook of Microwave and Optical Components* (Wiley, 1989 and 1990), the Wiley Microwave and Optical Engineering Book Series, and *Microwave and Optical Technology Letters*. He has also published over 250 technical papers and several book chapters in the areas of microwave and millimeter-wave devices, circuits, and antennas. His current interests are in microwave and millimeter-wave devices and circuits, microwave integrated circuits, integrated antennas, wide-band and active antennas, phased arrays, power transmission, and microwave optical interactions.

Dr. Chang received the Special Achievement Award from TRW and the Halliburton Professor Award (1988), the Distinguished Teaching Award (1989), the Distinguished Research Award (1992), and the TEES Fellow Award (1996) from Texas A&M University.